Bioinformatic analysis and experimental validation of six cuproptosis-associated genes as a prognostic signature of breast cancer

Xiang Chen [Equal first author, 1] , **Hening Sun** [Equal first author, 1] , **Changcheng Yang** [2] , **Wei Wang** [1] , **Wenzhi Lyu** [1] , **Kejian Zou** [1] , **Fan Zhang** [1] , **Zhijun Dai** [3] , **Xionghui He** [Corresp., 1] , **Huaying Dong** [Corresp. 1]

[1] Department of Hainan General Hospital, Hainan Medical College, Haikou City, Hainan Province, China

[2] Department of The First Affiliated Hospital, Hainan Medical College, Haikou City, Hainan Province, China

[3] Department of The First Affiliated Hospital, Zhejiang University, Hangzhou City, Zhejiang Province, China

Corresponding Authors: Xionghui He, Huaying Dong
Email address: hxh7582@163.com, dr_dhy@163.com

Background: Breast carcinoma (BRCA) is a life-threatening malignancy in women and shows a poor prognosis. Cuproptosis is a novel mode of cell death but its relationship with BRCA is unclear. This study attempted to develop a cuproptosis-relevant prognostic gene signature for BRCA. **Methods:** Cuproptosis-relevant subtypes of BRCA were obtained by consensus clustering. Differential expression analysis was implemented using the 'limma' package. Univariate Cox and multivariate Cox analyses were performed to determine a cuproptosis-relevant prognostic gene signature. The signature was constructed and validated in distinct datasets. Gene set variation analysis (GSVA) and Gene set enrichment analysis (GSEA) were also conducted using the prognostic signature to uncover the underlying molecular mechanisms. ESTIMATE and CIBERSORT algorithms were applied to probe the linkage between the gene signature and tumor microenvironment (TME). Immunotherapy responsiveness was assessed using the Tumor Immune Dysfunction and Exclusion (TIDE) web tool. Real-time quantitative PCR (RT-qPCR) was performed to detect the expressions of cuproptosis-relevant prognostic genes in breast cancer cell lines.
Results: Thirty-eight cuproptosis-associated differentially expressed genes (DEGs) in BRCA were mined by consensus clustering and differential expression analysis. Based on univariate Cox and multivariate Cox analyses, six cuproptosis-relevant prognostic genes, namely SAA1, KRT17, VAV3, IGHG1, TFF1, and CLEC3A, were mined to establish a corresponding signature. The signature was validated using external validation sets. GSVA and GSEA showed that multiple cell cycle-linked and immune-related pathways along with biological processes were associated with the signature. The results ESTIMATE and CIBERSORT analyses revealed significantly different TMEs between the two Cusig score subgroups. Finally, RT-qPCR analysis of cell lines further confirmed the expressional trends

of SAA1, KRT17, IGHG1, and CLEC3A. **Conclusion:** Taken together, we constructed a signature for projecting the overall survival of BRCA patients and our findings authenticated the cuproptosis-relevant prognostic genes, which are expected to provide a basis for developing prognostic molecular biomarkers and an in-depth understanding of the relationship between cuproptosis and BRCA.

1 **Bioinformatic analysis and experimental validation of six cuproptosis-**

2 **associated genes as a prognostic signature of breast cancer**

4 Xiang Chen[1†], Hening Sun[1†], Changcheng Yang[2], Wei Wang[1], Wenzhi Lyu[1], Kejian Zou[1], Fan

5 Zhang[1], Zhijun Dai[3], Xionghui He[1*], Huaying Dong[1*]

6 1. Department of General Surgery, Hainan General Hospital, Hainan Affiliated Hospital of

7 Hainan Medical University, 570311, Haikou, China.

8 2. Department of Medical Oncology, The First Affiliated Hospital of Hainan Medical University,

9 570102, Haikou, China.

10 3. Department of Breast Surgery, The First Affiliated Hospital, School of Medicine, Zhejiang

11 University, Hangzhou, 310003, China.

12 * Correspondence: dr_dhy@163.com; hxh7582@163.com.

13 † These authors contributed equally: Xiang Chen and Hening Sun.

15 **Abstract**

16 **Background:** Breast carcinoma (BRCA) is a life-threatening malignancy in women and shows a

17 poor prognosis. Cuproptosis is a novel mode of cell death but its relationship with BRCA is

18 unclear. This study attempted to develop a cuproptosis-relevant prognostic gene signature for

19 BRCA.

20 **Methods:** Cuproptosis-relevant subtypes of BRCA were obtained by consensus clustering.

21 Differential expression analysis was implemented using the 'limma' package. Univariate Cox

22 and multivariate Cox analyses were performed to determine a cuproptosis-relevant prognostic

23 gene signature. The signature was constructed and validated in distinct datasets. Gene set

24 variation analysis (GSVA) and Gene set enrichment analysis (GSEA) were also conducted using

25 the prognostic signature to uncover the underlying molecular mechanisms. ESTIMATE and

26 CIBERSORT algorithms were applied to probe the linkage between the gene signature and

27 tumor microenvironment (TME). Immunotherapy responsiveness was assessed using the Tumor

28 Immune Dysfunction and Exclusion (TIDE) web tool. Real-time quantitative PCR (RT-qPCR)

29 was performed to detect the expressions of cuproptosis-relevant prognostic genes in breast

30 cancer cell lines.

31 **Results:** Thirty-eight cuproptosis-associated differentially expressed genes (DEGs) in BRCA

32 were mined by consensus clustering and differential expression analysis. Based on univariate

33 Cox and multivariate Cox analyses, six cuproptosis-relevant prognostic genes, namely SAA1,

34 KRT17, VAV3, IGHG1, TFF1, and CLEC3A, were mined to establish a corresponding signature.

35 The signature was validated using external validation sets. GSVA and GSEA showed that

36 multiple cell cycle-linked and immune-related pathways along with biological processes were

37 associated with the signature. The results ESTIMATE and CIBERSORT analyses revealed

38 significantly different TMEs between the two Cusig score subgroups. Finally, RT-qPCR analysis

39 of cell lines further confirmed the expressional trends of SAA1, KRT17, IGHG1, and CLEC3A.

40 **Conclusion:** Taken together, we constructed a signature for projecting the overall survival of

41 BRCA patients and our findings authenticated the cuproptosis-relevant prognostic genes, which

42 are expected to provide a basis for developing prognostic molecular biomarkers and an in-depth

43 understanding of the relationship between cuproptosis and BRCA.

44   **Keyword:** breast carcinoma; cuproptosis; prognostic signature; tumor microenvironment

45   **Introduction**

46   Breast carcinoma (BRCA) is the most common malignancy and the second leading cause of

47   cancer-related deaths among women (1). In most Asian countries, BRCA is a malignancy that

48   threatens women's lives (2), and its incidence is increasing more rapidly compared to Western

49   countries (2,3). Based on the expression of hormone and cell membrane receptors, BRCA can be

50   divided into four subtypes, namely luminal A-like, luminal B-like, HER2 positive, and triple-

51   negative breast cancer (TNBC) (4). TNBC lacks expression of all three receptors and is an

52   aggressive malignancy with a poor prognosis, accounting for 10–20% of all BRCA cases (5).

53   Clinically, some BRCA treatments, like mastectomy, chemotherapy, and radiotherapy, have

54   serious side effects (6). Chemotherapy is more effective than mastectomy and radiotherapy for

55   metastatic cancer (7); however, conventional chemotherapeutic drugs are associated with serious

56   side effects such as neutropenia, stomatitis, and mucositis (8). Nanoparticle-based cancer

57   vaccines are currently being developed and are in the early stages (9). Therefore, although the

58   prognosis of many BRCA patients has improved with the existing medical technology, due to

59   individual differences, the clinical markers of tumor grade, tumor size, and TNM stage alone are

60   far from satisfactory for personalised diagnosis and treatment. Moreover, many BRCA patients

61   are still at risk of recurrence and death (10,11). There is therefore a need to develop new

62   molecular prognostic markers and related therapeutic agents to achieve more precise treatment.

63   A recent study found that various copper ion carrier drugs such as elesclomol (ES),

64   disulfiram, and NSC319726 can cause cell death. This copper-induced cell death or cuproptosis

65   is a novel form that differs from other programmed cell death types (e.g. apoptosis, pyroptosis,

66   necrosis, and ferroptosis) (12). Copper ions are necessary for all living things, including bacteria,

67   animals, and humans. These also play a crucial role in biological processes as cofactors for key

68   enzymes. While under normal physiological conditions, copper ions are kept at low

69   concentrations in a state of dynamic equilibrium in living things, their excessive buildup may

70   result in copper toxicity, which in turn can cause cell death. Further investigation into the

71   potential cause of cuproptosis has revealed that copper ions can bind to thioctylated proteins in

72   the tricarboxylic acid (TCA) cycle, contributing to abnormal oligomerization of thioctylated

73   proteins and reduced Fe-S cluster protein levels, both of which cause a proteotoxic stress

74   response that ultimately results in cell death. In addition, previous studies have shown that

75   copper-chelating drugs can significantly increase the number of infiltrating CT8$^+$ T and natural

76   killer cells in tumor cells while reducing the growth rate of tumor cells (13). Recent studies have

77   shown that cuproptosis-related genes are involved in numerous immune-related pathways in

78   BRCA, whereby there is a heavy infiltration of CD4$^+$, activated NK cells, memory T cells,

79   macrophages, and CD8 T cells (14-16).

80   However, reports on cuproptosis in BRCA are relatively rare. In this study, we identified

81   cuproptosis-relevant genes and their prognostic value in BRCA by bioinformatics and assessed

82   the relationship between cuproptosis-relevant prognostic features and tumor microenvironment

83   and immune cell infiltration. The findings are expected to facilitate the development of new

84   treatment strategies for BRCA.

85   **Material and methods**

86   **Data sources**

87   The Cancer Genome Atlas (TCGA)-BRCA cohort comprising sequencing data and clinical

88   information of 1091 BRCA samples and 113 normal samples, was acquired from TCGA

89   database (https://xenabrowser.net). Of these, 1069 BRCA samples with survival information

90   (after filtering out samples without details of age, M, N, T, and stage) were incorporated into the

91   survival analysis. GSE42568 and GSE20711 cohorts were retrieved from the Gene Expression

92   Omnibus (GEO) database (https://www.ncbi.nlm.nih.gov/geo/query/acc.cgi?acc=GSE42568)

93   and employed as external validation sets for assessing the cuproptosis-relevant prognostic

94   signature. GES42568 and GSE20711 cohorts included 104 and 88 BRCA samples with

95   corresponding survival information and data, respectively. The RNA-seq FPKM data of TCGA-

96   BRCA cohort and GSE42568 dataset were normalized with log2 (FPKM+1) values. Ten

97   cuproptosis-relevant genes (FDX1, LIAS, LIPT1, DLD, DLAT, PDHA1, PDHB, MTF1, GLS,

98   and CDKN2A) were extracted from a previous study (12).

99   **Functional enrichment analysis**

100 The online website DAVID (https://david.ncifcrf.gov/) (17,18) and the R package

101 'clusterProfiler' (19) were employed for Gene Ontology (GO) and Kyoto Encyclopedia of Genes

102 and Genomes (KEGG) enrichment analyses (20). GO terms were annotated as cellular

103 component (CC), molecular function (MF), and biological process (BP).

104 **Identifying BRCA-related subtypes**

105 BRCA cases in TCGA-BRCA cohort were classified based on the expression of corresponding

106   genes by consensus clustering using the 'ConsensusClusterPlus' package (21). The consensus

107   matrix and consensus CDF curve were generated for selecting the optimal typing. Uniform

108   manifold approximation and projection (UMAP) maximized the retention of features of the

109   original data while reducing the feature dimensionality and was used to conduct dimensional

110   reduction analysis on different subtypes.

111   **Differential expression analysis**

112   Depending on p-value < 0.05 and $|\log_2\text{FoldChange(FC)}| > 0.5$, we obtained differentially

113   expressed genes (DEGs) using the 'limma' package (22).

114   **Tumor microenvironment (TME) analysis**

115   The 'estimate' package in R was utilized to compute the immune, stromal, and ESTIMATE

116   scores, along with tumor purity for each BRCA sample (23). Using the ssGSEA (24) and

117   CIBERSORT algorithms (25), immune gene sets and the fraction of immune infiltrating cells

118   were calculated for each BRCA sample.

119   **Establishing cuproptosis-relevant prognostic signature in BRCA**

120   First, we acquired genes that were significantly associated with OS of BRCA patients by

121   univariate Cox analysis. Subsequently, we calculated the two principal components, PC1 and

122   PC2, for each sample. The PC1 and PC2 values were subjected to multivariate Cox regression

123   analysis to obtain corresponding coefficients; according to the formula, Cusig score $= \Sigma$

124    $(PC1_i + PC2_i)$, where i represents the expression of genes, we calculated the Cusig score of each

125   BRCA sample. The surv cutpoint function of the 'survminer' package was used to obtain the

126   optimal cutoff value to classify BRCA patients into the high-CuSig score and low-CuSig score

127 groups.

Enrichment analysis of pre-defined gene sets based on the prognostic signature

129 Gene set variation analysis (GSVA) was implemented through the 'gsva' package in R (24,26)

130 and 'c2.cp.kegg.v7.2.symbols.gmt' and 'h.all.v7.5.1.symbols.gmt' were the reference gene sets.

131 Differential HALLMARK/KEGG entries were then obtained using the 'limma' package, and the

132 filtering criteria were $|\log_2 FC| > 0.1$ and p-value < 0.05. Gene set enrichment analysis (GSEA)

133 was also conducted by setting the GO gene set as the reference. The threshold values for

134 significant entries were SIZE > 20 and NOM p-value < 0.05.

Immunotherapy efficacy analysis based on the prognostic signature

136 The sensitivity of the two Cusig score subgroups to immune checkpoint blockade (ICB) therapy

137 was inferred and assessed on the Tumor Immune Dysfunction and Exclusion (TIDE) website

138 (27). The calculated TIDE value was used for evaluating the efficacy of immunotherapy.

Assessing mRNA expressions of cuproptosis-relevant prognostic genes in cell lines

140 The RT-qPCR validation was performed and reported according MIQE guidelines (28). A

141 human epithelial cell line from the mammary gland, MCF-10A (normal group), and three breast

142 cancer cell lines, HCC1937, MCF-7, and MDA-MB-231 (BRCA group), were acquired from

143 iCell Bioscience Inc (Shanghai, China) , of which MCF-10A, MCF7 and MDA-MV-231 cells

144 were cultured in one plate, and HCC1937 cells were cultured in three plates. MCF-10A cells

145 were cultured in MEGM Kit medium (Lonza/Clonetics, CC-3150). HCC1937 cells were cultured

146 in RPMI-1640 medium (iCell-0002) supplemented with 10% fetal bovine serum (FBS) (Gibco)

147 and 1% penicillin/streptomycin. MCF-7 cells were cultured in MEM basic medium (iCell-0012)

148   supplemented with 0.01 mg/mL of bovine insulin, 10% FBS, and 1% penicillin/streptomycin.

149   MDA-MB-231 cells were cultured in L15 medium (iCell-0009) supplemented with 10% FBS

150   (Gibco) and 1% penicillin/streptomycin. The cells were incubated at 37°C in an atmosphere with

151   5% CO_2. Total RNA from the four cell lines in the logarithmic phase was extracted using the

152   TRIzol Reagent following the manufacturer's instructions (Ambion, USA). Chloroform

153   (Chengdu Guerda rubber industry Co., LTD, Chengdu, China) was used to remove proteins and

154   fat-soluble magazines, ice isopropanol (Chengdu Guerda rubber industry Co., LTD, Chengdu,

155   China) was used to precipitate RNA, and 75% ethanol (Chengdu Colon Chemical Co., LTD,

156   Chengdu, China) was used to further remove impurities. Subsequently, 20-50 μL of RNase-free

157   water (Servicebio, Guangzhou, China) was added to the obtained RNA precipitate to solubilize

158   the RNA and the RNA concentration was detected with NanoPhotometer N50. Next, total RNA

159   was reverse transcribed into cDNA using the SweScript-First-strand-cDNA-synthesis-kit

160   (Servicebio, Guangzhou, China) and the reaction system was made up of 4 μL of 5xReaction

161   Buffer, 1μL of primer, 1μL of SweScript RT I Enzyme Mix, 0.1ng-5μg of total RNA, and

162   nuclease-free water replenished to 20 μL. Afterthat, the qPCR was performed using the

163   2xUniversal Blue SYBR Green qPCR Master Mix following the manufacturer's direction

164   (Servicebio, Guangzhou, China) with the reaction system of 3 μL cDNA, 5 μL 2xUniversal Blue

165   SYBR Green qPCR Master Mix and 1 μL each upstream and downstream primers. Finally, the

166   reactions were performed on a CFX96 real-time quantitative fluorescence PCR instrument. The

167   amplification reactions were programmed with pre-denaturation at 95 °C for 1 min, followed by

168   40 cycles, each cycle consisting of 95 °C for 20 s, 55 °C for 20 s, and 72 °C for 30 s. The relative

169   expression of genes was calculated by the 2−ΔΔCt method using GADPH as the internal

170   reference gene. P-value was calculated by Graphpad Prism 5, and p less than 0.05 was

171   considered to have statistical difference. The sequences of the primers used in this study are

172   presented in **Table 1**, and the concentration of primer was 10 μM. The amplicon size was 80-350

173   bp.

174   **Statistical analysis**

175   Kaplan-Meier (KM) curves were generated using the 'survminer' package (prognostic model

176   survival analysis) and the 'survival' package. The somatic mutation analysis and visualization

177   were using the 'maftools' package in R. All bioinformatics analyses were undertaken in R

178   language. The Wilcoxon test (comparison between two groups), Kruskal-Wallis test (comparison

179   between three or more groups), and chi-square test (correlation analysis between cuproptosis-

180   relevant subtypes and clinical factors) were employed to compare the data from different groups.

181   Unless specified, a p-value < 0.05 was considered statistically significant.

182   **Results**

183   **Expression of ten cuproptosis-relevant genes in BRCA**

184   First, we conducted the functional enrichment analysis of 10 cuproptosis genes (FDX1, LIAS,

185   LIPT1, DLD, DLAT, PDHA1, PDHB, MTF1, GLS, and CDKN2A) using the DAVID web tool.

186   As shown in **Figs.1A-B**, 11 GO entries (5 BP, 4 CC, and 2 MF) and 8 KEGG pathways were

187   enriched. These genes were involved in 'acetyl-CoA biosynthetic process from pyruvate',

188   'mitochondrial acetyl-CoA biosynthetic process from pyruvate', 'tricarboxylic acid cycle',

189   'glucose   metabolic   process',   'protein   lipoylation',   'pyruvate   metabolism',

190   'glycolysis/gluconeogenesis', 'carbon metabolism', 'metabolic pathways', 'central carbon

191   metabolism in cancer', 'lipoic acid metabolism' and 'biosynthesis of cofactors'. The locations of

192   these 10 cuproptosis genes on the chromosomes are exhibited in the circle diagram

193   (**Supplementary Figure 1**). Somatic mutation analysis of 986 samples with somatic mutation

194   information from TCGA-BRCA cohort revealed a very low mutation rate of the 10 cuproptosis

195   genes in BRCA (**Fig.1C**). Further analysis of transcriptomic data from TCGA-BRCA cohort

196   revealed that the expressions of CDKN2A and PDHB were significantly elevated, and those of

197   DLAT, DLD, FDX1, GLS, LIAS, LIPT1, MTF1, and PDHA1 was significantly lowered in

198   BRCA samples compared to normal samples (**Fig.1D**).

199   **Identification of cuproptosis-associated subtypes of BRCA**

200   Consensus clustering was implemented to identify BRCA-related subtypes, and 1091 BRCA

201   patients in TCGA-BRCA cohort were categorized into cuproptosis-associated subtypes based on

202   the expression of 10 cuproptosis genes. Optimal clustering stability was confirmed at K = 3

203   (**Supplementary Figure 2A-C**). Clusters 1, 2, and 3 included 473, 296, and 322 samples,

204   respectively. UMAP reduced dimensional analysis demonstrated that the samples of cluster 1

205   and cluster 2 were distributed separately and could be well distinguished (**Fig.2A**). Survival

206   analysis revealed significantly higher OS for patients in cluster 1 than in cluster 2 (P = 0.03688)

207   (**Fig.2B**). By chi-square tests, we examined the correlation between three cuproptosis-associated

208   subtypes and clinical factors. The results showed that the three subtypes were significantly

209   associated with age, race, and N stage but not with T stage, M stage, and stage (**Figs.2C-H**). To

210   further explore the discrepancies in the TMEs of the three cuproptosis-associated subtypes, we

211   first calculated and compared the immune scores, stromal scores, estimate scores, and tumor

212   purity across the three subtypes. As shown in **Figs.3A-D**, the stromal scores of all three subtypes

213   were significantly different. The immune score, stromal score, and estimate score of cluster 1

214   and cluster 2 were significantly higher than those of cluster 3, and the tumor purity of cluster 1

215   and cluster 2 was significantly lower than that of cluster 3. Using the ssGSEA algorithm and

216   Kruskal-Wallis test, we calculated and compared 28 immune gene sets across the three subtypes

217   to further assess their differential immune activities. As shown in **Figs.3E-F**, all 28 immune gene

218   sets differed significantly among the three subtypes. To further compare the differences in

219   fractions of immune cell infiltrates among the three subtypes, we employed the CIBERSORT

220   algorithm and performed the Kruskal-Wallis test. The infiltration levels of a total of 14 immune

221   cell types differed significantly among the three subtypes, including naïve B cells, memory B

222   cells, activated dendritic cells, macrophages M1, macrophages M2, resting mast cells,

223   neutrophils, activated NK cells, resting NK cells, resting CD4 memory T cells, activated CD4

224   memory T cells, CD8 T cells, follicular helper T cells, and regulatory T cells (Tregs) (**Fig.3G**).

225   **Cuproptosis-associated DEGs in BRCA**

226   To authenticate the cuproptosis-associated DEGs in BRCA, we first identified the DEGs

227   between BRCA and normal samples, between cluster 1 and cluster 2, between cluster 2 and

228   cluster 3, and between cluster 1 and cluster 3. A total of 4878 DEGs (2441 up-regulated and

229   2437 down-regulated genes) between BRCA and normal samples, 581 DEGs (270 up-regulated

230   and 311 down-regulated genes) between cluster 1 and cluster 2, 705 DEGs (433 up-regulated and

231   272 down-regulated genes) between cluster 2 and cluster 3, and 1221 DEGs (598 up-regulated

232 and 623 down-regulated genes) between cluster 1 and cluster 3 were identified. By taking the

233 intersection of the above four groups of DEGs using a Venn diagram, 38 common genes were

234 defined as cuproptosis-associated DEGs in BRCA (**Fig.4A**, **Supplementary Table 1**). The

235 results of Pearson correlation analysis between the 38 intersecting genes and 10 cuproptosis

236 genes are shown in Figure 4B. To further probe the function of these 38 genes in BRCA, a

237 functional enrichment analysis was conducted. As shown in **Supplementary Table 2**, 18 GO

238 terms (13 BP, 2 CC, and 3 MF) and 1 KEGG pathway were significantly enriched. The top10

239 items under each classification are shown in a bar diagram (**Fig.4C**). The abovementioned genes

240 were mainly linked to 'response to iron ion', 'response to estradiol', 'response to estrogen',

241 'response to xenobiotic stimulus', 'neutrophil chemotaxis', 'response to drug', 'hormone

242 metabolic process', 'mammary gland alveolus development', and 'estrogen signaling pathway'.

243 We categorized the 1091 BRCA patients in TCGA-BRCA cohort into five subtypes based on the

244 expression of 38 cuproptosis-associated DEGs in BRCA and consensus clustering

245 (**Supplementary Figure 3A-C**). Clusters 1, 2, 3, 4, and 5 consisted of 225, 178, 210, 320, and

246 158 samples, respectively. The distribution of clinical features of the five subtypes and the

247 expression of 38 cuproptosis-associated DEGs are shown as a heatmap (**Fig.4D**). Survival

248 analysis revealed no significant survival discrepancies among the five subtypes (Chisq = 6, df =

249 4, p = 0.2) (**Fig.4E**).

250 **Cuproptosis-relevant prognostic signature for BRCA**

251 To establish a cuproptosis-relevant prognostic signature, we first identified six genes

252 significantly associated with OS in BRCA patients among the 38 cuproptosis-associated DEGs in

253   BRCA using univariate Cox analysis, namely SAA1, KRT17, VAV3, IGHG1, TFF1, and

254   CLEC3A (**Fig.5A**). Next, we performed a principal component analysis for the above six genes

255   and calculated the PC1 and PC2 values for each BRCA sample (**Supplementary Table 3**). The

256   coefficients of PC1 and PC2 values were obtained by multivariate Cox regression analysis.

257   According to the formula, Cusig score = 0.087984*PC1 value + 0.226539*PC2 value, we

258   calculated the Cusig score for each BRCA sample and subsequently categorized the BRCA

259   patients into the high-Cusig score group (552 cases) and low-CuSig score group (517 cases)

260   according to the optimal cut-off value (0.9889137). The KM curve suggested that the survival of

261   the patients in the high-Cusig score group was significantly worse than that of the low-Cusig

262   score group (**Fig.5B**). The Sankey diagram exhibited the correlation between the different

263   subtypes and high- and low-Cusig scores (**Fig.5C**). The Cusig scores were also significantly

264   different between the five BRCA subtypes based on 38 cuproptosis-associated DEGs in BRCA

265   (**Fig.5D**). Cluster 2, which had a better prognosis, had a lower Cusig score, compared to the

266   other clusters (**Figs.4E, 5D**). We further validated the Cusig score model in external datasets,

267   GSE42568 and GSE20711, and similarly, the high-Cusig score group showed a significantly

268   worse prognosis than the low-Cusig score group, consistent with the results of TCGA-BRCA

269   cohort (**Figs.5E-F**).

270   **Uncovering the molecular mechanisms of cuproptosis-relevant prognostic signature**

271   **underlying BRCA**

272   In order to uncover potential mechanisms underlying the differential prognoses between the two

273   Cusig score subgroups, GSVA was conducted to analyze the enrichment differences in the terms

274 of KEGG and hallmark pathways between different Cusig score groups. As shown in

275 **Supplementary Table 4** and **Figs.6A-B**, 22 hallmark pathways and 73 KEGG pathways were

276 enriched. 'E2F targets', 'G2M checkpoint', 'protein secretion', 'unfolded protein response',

277 'MTORC1 signaling', 'MYC targets V1', and 'DNA repair' were enriched in the high-Cusig

278 score group (**Fig.6A**). 'Citrate cycle', 'TCA cycle', 'RNA degradation', 'cell cycle' and 'DNA

279 replication' were also enriched in the high-Cusig score group (**Fig.6B**). Immune-related hallmark

280 pathways, like 'IL2-STAT5 signaling', 'inflammatory response', 'IL6-JAK-STAT3 signaling',

281 'TNFA signaling via NFKB', and KEGG pathways, including 'chemokine signaling pathway',

282 'NOD-like receptor signaling pathway', 'TGF-β signaling pathway', 'complement and

283 coagulation cascades', 'natural killer cell-mediated cytotoxicity', 'cytokine-cytokine receptor

284 interaction', and 'B cell receptor signaling pathway' were enriched in low-Cusig score group

285 (**Figs.6A-B**). Next, we screened DEGs of the Cusig score subgroups and conducted GO

286 functional enrichment analysis. As shown in **Supplementary Table 5,** 1289 GO entries (1152

287 BP, 67 CC, and 70 MF) were derived based on 590 DEGs between the high- and low-Cusig

288 score groups. The top 10 GO-BP terms are shown in **Fig.6C**. Immune-related and cell adhesion-

289 related BPs were associated with these DEGs. The results of GSEA indicated that 484 and 1686

290 GO entries (NES > 0 and NES < 0, respectively) were enriched in the high-Cusig and low-Cusig

291 score groups, respectively (**Supplementary Table 6**). The top 5 enriched entries of the two

292 Cusig score subgroups are shown in **Fig.6D**. Notably, mitosis-related and DNA replication-

293 related BPs were closely associated with the high-Cusig score group, and multiple immune-

294 related BPs were closely associated with the low-Cusig score group.

Association of cuproptosis-relevant prognostic signature with TME

Since immune-related pathways and BPs were found to be associated with the low-Cusig score group, we next analyzed the relationship between the Cusig score and TME and immune cell infiltration. The ESTIMATE algorithm demonstrated that patients with low Cusig scores had higher immune scores, stromal scores, estimate scores, and lower tumor purity **(Figs.7A-D)**. The results of the CIBERSORT algorithm showed that the fractions of naïve B cells, plasma cells, CD8 T cells, monocytes, resting dendritic cells, eosinophils, and neutrophils were elevated in the patients with lower Cusig scores, while the fractions of macrophages M0 and macrophages M2 were high in the patients with high Cusig scores (**Fig.7E**). Moreover, PD-L1 expression and immunophenoscore (IPS) of the low-Cusig score group were higher than those of the high-Cusig score group (**Figs.7F-G**). However, the results of the TIDE analysis showed that the high-Cusig score group had a lower TIDE score than the low-Cusig score group and these patients may be more sensitive to ICB therapy (**Fig.7H**).

The mutational landscape of high- and low-Cusig score samples

To further assess the mutation frequency of genes in high- and low-Cusig score samples, we performed somatic mutation analysis. The most frequently mutated genes in the high-Cusig score and low-Cusig score samples were TP53 and PIK3CA, respectively (**Figs.8A-B**). The top 20 mutated genes were not identical between the two Cusig score subgroups, indicating different somatic mutation patterns (**Fig.8A-B**). We then analyzed the copy number variation (CNV) in genes of the two Cusig score subgroups and found that the CNV of genes in the low-Cusig score samples was significantly higher than that in the high-Cusig score samples (**Fig.8C**).

316   **Expression of cuproptosis-relevant prognostic genes in BRCA**

317   As shown in **Supplementary Figure 4,** CLEC3A, IGHG1, TFF1, and VAV3 were up-regulated,

318   while KRT17 and SAA1 were down-regulated in BRCA tissues compared to normal tissues in

319   TCGA-BRCA cohort. We then checked the expression of prognostic genes at the mRNA level in

320   the human epithelial cell line from the mammary gland, MCF-10A, and three breast cancer cell

321   lines HCC1937, MCF7, and MDA-MB-231. Consistent with the trend of results from public

322   databases, levels of CLEC3A and IGHG1 were up-regulated, while those of KRT17 and SAA1

323   were down-regulated in breast cancer cell lines (**Fig.9**). The amplification and dissolution curves

324   of prognostic genes were displayed in **Supplementary Table 7**. However, inconsistent with the

325   results from the tissue samples, TFF1 and VAV3 were down-regulated in breast cancer cell lines

326   (**Fig.9, Supplementary Table 7**). The amplification and dissolution curves of prognostic genes

327   were displayed in **Supplementary Table 8**. However, inconsistent with the results from the

328   tissue samples, TFF1 and VAV3 were down-regulated in breast cancer cell lines (**Fig.9**),

329   probably due to the complexity of the tumor tissue.

330   **Discussion**

331   Much progress has been made in research on BRCA but it remains one of the most common

332   cancers seriously affecting women's health. The incidence and mortality of BRCA will continue

333   to increase in the coming years (29). Cuproptosis gained traction as a novel form of cell death,

334   and the dysregulation of copper, an indispensable trace element in human homeostasis, may

335   trigger cytotoxicity (30). Copper levels are significantly elevated in cancer patients compared to

336   normal controls, and altered copper levels in cells can influence the development of cancer

337   (31,32). In this context, we investigated the prognostic value of cuproptosis-related genes in

338   BRCA as this is expected to facilitate the improvement of BRCA diagnosis and treatment.

339   In this study, we first performed a functional enrichment analysis of 10 cuproptosis genes in

340   BRCA. We found that most of these genes were involved in BPs 'acetyl-CoA biosynthetic

341   process from pyruvate', 'mitochondrial acetyl-CoA biosynthetic process from pyruvate', and

342   'tricarboxylic acid cycle', which are all closely linked to the development of BRCA (33). Among

343   the 10 cuproptosis genes, the expressions of CDKN2A and PDHB were dramatically increased in

344   BRCA samples compared to normal samples but those of the other genes decreased significantly.

345   The role of CDKN2A across tumor types appears to differ. CDKN2A regulates transcriptional

346   elongation to promote the progression of non-small cell lung cancer (34). CDKN2A promotes

347   proliferation and invasion in glioblastoma (35). CDKN2A is highly expressed in precancerous

348   lesions of the stomach while poorly expressed in gastric cancer (36). In BRCA, CDKN2A is

349   defined as a tumor suppressor gene, and our review of the literature suggests that this gene has a

350   low mutation rate in BRCA but a single mutation may significantly impact protein function (37).

351   A recent study showed similar results; interestingly, CDKN2A was overexpressed in BRCA (38),

352   however, its exact mechanism of action remains unknown. The trend of expression of this gene

353   in BRCA is consistent with our findings. PDHB has been poorly studied in BRCA, and we can

354   only speculate on its functional role in BRCA based on its role in other cancers. Previously, on

355   the one hand, PDHB activity in pancreatic cancer cells was enhanced and accelerated the growth

356   of tumor cells (39). In retinoblastoma, overexpression of PDHB enhances tumor cell

357   angiogenesis and the inflammatory response, thereby promoting tumor development (40). On the

358   other hand, PDHB overexpression induces endoplasmic reticulum stress, which in turn inhibits

359   the proliferation and invasion of colorectal cancer cells, and in lung and gastric cancers (40,41).

360   We speculate that the expressional profile of PDHB at the transcriptional and protein levels may

361   be different across cancer types. In the present study, PDHB expression was high in BRCA

362   samples, and we speculate that it may function as an oncogene in breast cancer but the exact

363   mechanism of action needs further investigation. DLD is lowly expressed in a variety of human

364   cancer cells and is strongly associated with poor survival outcomes (42). FDX1 plays an

365   important role in protein esterification, and its low expression is associated with poor prognosis

366   in hepatocellular carcinoma (43). The specific mechanism of FDX1 action in BRCA needs to be

367   explored further. GLS catabolizes glutamine to glutamate, which is detrimental because

368   glutamine is rapidly absorbed and promotes the tumor growth of malignant tumors (44).

369   Interestingly, GLS expression is typically high in breast tumor tissues and is linked to a poor

370   prognosis (45). LIAS is primarily involved in the production of enzymes for mitochondria-

371   related metabolism, and high expression of LIAS promotes immune cell infiltration and is linked

372   to improved survival in BRCA (46,47). Although LIPT1 has a major role in TCA-related

373   metabolism (48), its exact mode of action in BRCA is unknown. According to recent research,

374   LIPT1 prevents cell migration in bladder cancer (49). In melanoma, it may prevent tumor growth

375   by interfering with the mitochondrial TCA and causing copper dystrophy (50). Combined with

376   our findings, this supports the possibility that LIPT1 may operate as a protective factor in breast

377   cancer. MTF1 is a metal-regulated transcription factor that normally binds to zinc to activate its

378   DNA-binding region to bind designated target genes (51). Down-regulation of the upstream gene,

379   MTF1 in BRCA may reduce the activity of downstream genes, resulting in decreased cellular

380   activity (52). PDHA1 is involved in the regulation of glucose metabolic reprogramming in

381   BRCA cells and low expression of PDHA1 is detrimental to the prognosis of these patients

382   (53,54).

383   Next, we divided the patients into three subgroups based on the expression of the 10

384   cuproptosis genes in BRCA. These three subgroups showed significant differences in their TMEs,

385   with cluster 1 showing the highest levels of immune cell infiltration and cluster 3 showing the

386   opposite pattern. The role of TME and immune cell infiltration in the development of cancer is

387   well established (55). Significant immune cell infiltration occurs early in the development of the

388   tumor or before invasion occurs (56,57). In the late stage, low levels of immune cell infiltration

389   in TME often lead to a poorer prognosis (58), and this holds true in BRCA (59). In our study, OS

390   was significantly higher in cluster 1 than in cluster 3, suggesting a possible correlation between

391   immune cell infiltration and tumor stage in BRCA. Furthermore, the analysis of the level of

392   immune cell infiltration in the three subtypes showed that cluster 1 had significant infiltration of

393   memory B cells, CD8 T cells, follicular helper T cells, and activated NK cells. Cluster 3 showed

394   significant infiltration of immune cells such as resting mast cells, plasma cells, and macrophages

395   M2. Previous studies supported our finding that immune infiltrating cells in cluster 1 were

396   associated with a better survival prognosis in breast cancer, while the latter occurred more often

397   in advanced BRCA cases (60-62). Through the functional enrichment analysis of cuproptosis-

398   associated DEGs in BRCA, 38 cuproptosis-associated DEGs were found to be mainly associated

399   with 'response to iron ion', 'response to estradiol', 'response to estrogen', 'response to

400 xenobiotic stimulus', 'neutrophil chemotaxis', 'response to drug', 'hormone metabolic process',

401 'mammary gland alveolus development', and 'estrogen signaling pathway'. A few studies have

402 shown that these BPs are involved in the development of BRCA (63-69).

403 Subsequently, we established a cuproptosis-associated prognostic signature based on

404 cuproptosis-associated DEGs linked to the prognosis of BRCA (SAA1, KRT17, VAV3, IGHG1,

405 TFF1, and CLEC3A). In BRCA, SAA1 knockdown induces cellular stress and fails to activate

406 the relevant molecular mechanisms involved in DNA as well as underlying BPs, which may be

407 more favorable for cancer cell survival (70). SAA1 overexpression in BRCA may be associated

408 with longer disease-free survival (71). KRT17 can promote carcinogenesis in several cancers

409 (72-74). The expression of KRT17 affects the phenotype of TNBC and can regulate tumor

410 differentiation through specific regulatory axes (75). In addition, KRT17 is a member of the

411 skeleton protein family, and when it is highly expressed, it can increase cell adhesion, thus

412 making the cell structure more stable and less prone to migration (76). The expression of KRT17

413 is higher in primary melanoma than in metastatic melanoma (77). Therefore, patients with high

414 KRT17 expression may have a better prognosis. VAV3 is an oncogenic gene that is

415 overexpressed in human BRCA and can promote its development by activating specific signaling

416 pathways and related genes. Silencing VAV3 impairs the growth of estrogen-stimulated and non-

417 dependent BRCA cells (78,79). Although BRCA samples have a high level of IGHG1 expression

418 (80), its precise mode of action is unknown. In other cancers, IGHG1 is linked to

419 immunoglobulins made by the cancer cells and plays a key role in helping cancer cells grow and

420 divide (81,82). TFF1 is an estrogen-regulatory gene because of the typical estrogen response

421 element in its promoter (83). However, there is controversy regarding its mechanism of action in

422 BRCA. TFF1 is an informative marker of metastatic BRCA and its overexpression is associated

423 with poor prognosis (84). However, another study showed that high TFF1 levels were associated

424 with better clinical outcomes, especially in early BRCA (85). Similarly, TFF1 not only has pro-

425 tumor properties but also exerts anti-tumor effects (86). Further studies are needed to assess its

426 role in tumor biology. CLEC3A is a risk gene among the cuproptosis-related prognostic genes

427 screened. Previous studies support our finding that CLEC3A is mainly involved in cellular

428 invasion and metastatic spread of BRCA. Silencing CLEC3A downregulates the activity of cell

429 survival factors and P13K/AKT, which reduces the proliferation, migration, and invasion of

430 BRCA cells (87,88). In conclusion, the genes screened herein may become new potential

431 therapeutic targets for BRCA.

432   Next, we created a Cusig score model by Cox regression analysis based on six cuproptosis-

433 associated prognostic genes, and as expected, the low Cusig score group was always associated

434 with a better prognosis as well as a higher survival rate, while the high Cusig score group

435 showed the opposite trend. To assess the causes more precisely, we performed GSVA and GSEA

436 to determine the potential underlying molecular mechanisms. Several immune-related BPs were

437 enriched in the low Cusig score group, while the high Cusig score group was significantly

438 enriched in pathways unrelated to the immune pathway. Previous cancer-related studies have

439 shown that KRAS signaling is associated with the progression of several cancers, such as non-

440 small cell lung cancer and pancreatic cancer (89,90). Our study showed that high KRAS

441 signaling was enriched in the low Cusig score group, which is consistent with previous results

442   showing that BRCA samples with high KRAS signaling tend to have higher infiltration of

443   immune cells such as CD8 cells and B cells; in other words, BRCA with high KRAS signaling

444   has a good tumor immune microenvironment and is associated with a better prognosis (91).

445   Angiogenesis is involved in the proliferation and metastasis of breast cancer and has even been

446   defined as a promising therapeutic target (92,93). In our study, angiogenesis was significantly

447   upregulated in the low Cusig score group, which seems contrary intuitively. We propose the

448   following hypothesis: most of the blood vessels on which more advanced BRCA cells depend for

449   growth are actually formed at an early stage and advanced BRCA cells do not require the

450   excessive formation of neovascularization for oxygen supply because the tumor cells themselves

451   have a low rate of oxygen consumption (94). This hypothesis has been reflected in previous

452   studies showing that tumors in advanced stages show less angiogenesis compared to early-stage

453   BRCA and that the dependence of tumor growth on neovascularization may be limited to early

454   stages (95). Epithelial-to-mesenchymal transition (EMT) showed a trend toward upregulation in

455   the low Cusig score group. EMT has been widely recognized as a critical driver of BRCA

456   (96,97). Notably, this pathway is localized at the level of primary tumor invasion, and as it

457   establishes secondary tumors at a distant site, it rapidly performs the reverse mesenchymal-

458   epithelial transition (MET) to rid itself of its mesenchymal attributes (98). This may explain our

459   results. A review of previous studies revealed that in breast cancer, the G2M checkpoint pathway

460   is significantly associated with tumor cell proliferation, similar to MYC targets v1 and E2F

461   targets and that tumors with high enrichment of the G2M checkpoint are more aggressive (99);

462   other studies have shown that the G2M checkpoint may be a promising therapeutic target for

463 improving the prognosis of BRCA patients (100). In conclusion, the above results are consistent

464 with our findings.

465   Finally, we analyzed the association between TME and the high and low Cusig score groups

466 in BRCA. B-cell subpopulations (including naïve B cells) were significantly increased in non-

467 metastatic BRCA and tumor metastasis may alter the function and phenotype of some of the B-

468 cell subpopulations, leading to their reduced proportions in advanced BRCA (101). Furthermore,

469 the role of eosinophils in tumors has been demonstrated, and there is an association between

470 higher eosinophil counts and a better prognosis (102). Indeed, the mechanism underlying its role

471 in BRCA remains unclear but in terms of expressional trends, this is consistent with our study.

472 Similarly, macrophages M0 and macrophages M2 are strongly associated with poor prognosis in

473 BRCA and may functionally mediate chemoresistance in BRCA (103). Immune checkpoint

474 inhibitors are a research hotspot. In BRCA, PD-L1 overexpression can inhibit the tumor-killing

475 effect of the autoimmune system. Clinically, drugs targeting the PD-1/PD-L1 axis have also been

476 used initially (104,105). In our study, PD-L1 expression was higher in the low Cusig score group,

477 which may be because the low Cusig score group possesses more immune-related mechanisms.

478   Previous studies have also created models that show good predictions (106) but we have

479 further validated our results using qPCR experiments, which demonstrates the reliability of our

480 findings. Additionally, as our analysis in this study was mostly bioinformatics-based, care should

481 be taken when interpreting the findings. We could only provide relationships in which functional

482 pathways play a role in TME processes and influence the prognosis of BRCA patients but we

483   have very limited evidence for a specific potential causal relationship, and this is the focus of our

484   future work.

485   **Conclusion**

486   In summary, herein, we constructed a signature for projecting the overall survival of BRCA

487   patients and our findings authenticated the cuproptosis-relevant prognostic genes, which are

488   expected to provide a basis for developing prognostic molecular biomarkers and an in-depth

489   understanding of the relationship between cuproptosis and BRCA.

490   **Acknowledgements**

491   Not applicable.

492   **Authors' contributions**

493   Huaying Dong, Xionghui He, and Zhijun Dai designed this work. Xiang Chen, Hening Sun, and

494   Changcheng Yang integrated and analyzed the data. Xiang Chen wrote this manuscript. Wei

495   Wang, Wenzhi Lyu, Kejian Zou, and Fan Zhang edited and revised the manuscript. All authors

496   approved this manuscript.

497   **Funding**

498   This work is supported by The Key Research and Development Program of Hainan Province

499   (ZDYF2021SHFZ055), Hainan Provincial Natural Science Foundation of China (822CXTD535)

500   and National Natural Science Foundation of China (81960475).

501   **Availability of data and materials**

502   All data used in this work can be acquired from the Gene-Expression Omnibus (GEO,

503   GSE42568, GSE20711; https://www.ncbi.nlm.nih.gov/geo/) and the GDC portal (https://

504   portal.gdc.cancer.gov/).

505   **Ethics approval and consent to participate**

506   Not applicable.

507   **Consent for publication**

508   Not applicable.

509   **Competing interests**

510   The authors declare that they have no competing interests.

511   **REFERENCES**

512   1.   Siegel RL, Miller KD, Fuchs HE, Jemal A. Cancer statistics, 2022. *CA A Cancer J Clinicians.*

513   2022;72(1):7-33.

514   2.   Mubarik S, Shakil Malik S, Wang Z, et al. Recent insights into breast cancer incidence trends

515   among four Asian countries using age-period-cohort model. *CMAR.* 2019;11:8145-8155.

516   3.   DeSantis CE, Ma J, Goding Sauer A, et al. Breast cancer statistics, 2017, racial disparity in

517   mortality by state. *CA: A Cancer Journal for Clinicians.* 2017;67(6):439-448.

518   4.   Goldhirsch A, Winer EP, Coates AS, et al. Personalizing the treatment of women with early

519   breast cancer: highlights of the St Gallen International Expert Consensus on the Primary

520   Therapy of Early Breast Cancer 2013. *Annals of Oncology.* 2013;24(9):2206–2223.

521   5.   Wahba HA, El-Hadaad HA. Current approaches in treatment of triple-negative breast cancer.

522   *Cancer Biol Med.* 2015;12(2):106-16.

523   6.   Miller KD, Siegel RL, Lin CC, et al. Cancer treatment and survivorship statistics, 2016. *CA:*

524   *A Cancer Journal for Clinicians*. 2016;66(4):271-89.

525   7. Chen J, Zhang X, Xiao X, et al. Xiao-Ai-Ping Injection Enhances Effect of Paclitaxel to

526   Suppress Breast Cancer Proliferation and Metastasis via Activating Transcription Factor 3.

527   *Integr Cancer Ther*. 2020;19:1534735420906463.

528   8. Hesketh PaulJ, Batchelor D, Golant M, et al. Chemotherapy-induced alopecia: psychosocial

529   impact and therapeutic approaches. *Support Care Cancer*. 2004;12(8):543-9.

530   9. Wen R, Umeano AC, Kou Y, Xu J, Farooqi AA. Nanoparticle systems for cancer vaccine.

531   *Nanomedicine*. 2019;14(5):627-648.

532   10. Zhang L, Cao J, Dong L, Lin H. TiPARP forms nuclear condensates to degrade HIF-1α and

533   suppress tumorigenesis. *Proc Natl Acad Sci USA*. 2020;117(24):13447–13456.

534   11. Bedenbender K, Scheller N, Fischer S, et al. Inflammation-mediated deacetylation of the

535   ribonuclease 1 promoter *via* histone deacetylase 2 in endothelial cells. *FASEB j.*

536   2019;33(8):9017–9029.

537   12. Tsvetkov P, Coy S, Petrova B, et al. Copper induces cell death by targeting lipoylated TCA

538   cycle proteins. *Science*. 2022;375(6586):1254-1261.

539   13. Voli F, Valli E, Lerra L, et al. Intratumoral Copper Modulates PD-L1 Expression and

540   Influences Tumor Immune Evasion. *Cancer Research*. 2020;80(19):4129–4144.

541   14. Li J, Wu F, Li C, et al. The cuproptosis-related signature predicts prognosis and indicates

542   immune microenvironment in breast cancer. *Front Genet*. 2022;13:977322.

543   15. Huang T, Liu Y, Li J, et al. Insights into prognosis and immune infiltration of cuproptosis-

544   related genes in breast cancer. *Front Immunol*. 2022;13:1054305.

545   16. Li W, Zhang X, Chen Y, Pang D. Identification of cuproptosis-related patterns and

546   construction of a scoring system for predicting prognosis, tumor microenvironment-

547   infiltration characteristics, and immunotherapy efficacy in breast cancer. *Front Oncol*.

548   2022;12:966511.

549   17. Sherman B T, Hao M, Qiu J, et al. DAVID: a web server for functional enrichment analysis

550   and functional annotation of gene lists (2021 update). *Nucleic Acids Research*.

551   2022;50(W1):W216-W221.

552   18. Huang DW, Sherman BT, Lempicki RA. Systematic and integrative analysis of large gene

553   lists using DAVID Bioinformatics Resources. *Nature Protoc*. 2009;4(1):44-57.

554   19. Wu T, Hu E, Xu S, et al. clusterProfiler 4.0: A universal enrichment tool for interpreting

555   omics data. *The Innovation*. 2021;2(3):100141.

556   20. Kanehisa M, Furumichi M, Tanabe M, Sato Y, Morishima K. KEGG: new perspectives on

557   genomes, pathways, diseases and drugs. *Nucleic Acids Res*. 2017;45(D1):D353–D361.

558   21. Wilkerson MD, Hayes DN. ConsensusClusterPlus: a class discovery tool with confidence

559   assessments and item tracking. *Bioinformatics*. 2010;26(12):1572-3.

560   22. Ritchie ME, Phipson B, Wu D, et al. limma powers differential expression analyses for

561   RNA-sequencing and microarray studies. *Nucleic Acids Research*. 2015;43(7):e47.

562   23. Yoshihara K, Shahmoradgoli M, Martínez E, et al. Inferring tumour purity and stromal and

563   immune cell admixture from expression data. *Nat Commun*. 2013;4:2612.

564   24. Hänzelmann S, Castelo R, Guinney J. GSVA: gene set variation analysis for microarray and

565   RNA-Seq data. *BMC Bioinformatics*. 2013;14:7.

566   25. Newman AM, Liu CL, Green MR, et al. Robust enumeration of cell subsets from tissue

567   expression profiles. *Nat Methods*. 2015;12(5):453-7.

568   26. Subramanian A, Tamayo P, Mootha VK, et al. Gene set enrichment analysis: A knowledge-

569   based approach for interpreting genome-wide expression profiles. *Proc Natl Acad Sci USA*.

570   2005;102(43):15545-50.

571   27. Jiang P, Gu S, Pan D, et al. Signatures of T cell dysfunction and exclusion predict cancer

572   immunotherapy response. *Nat Med*. 2018;24(10):1550-1558.

573   28. Bustin SA, Benes V, Garson JA, et al. The MIQE guidelines: minimum information for

574   publication of quantitative real-time PCR experiments. *Guideline*. 2009;55(4):611-22.

575   29. Greaney ML, Sprunck-Harrild K, Ruddy KJ, et al. Study protocol for Young & Strong: a

576   cluster randomized design to increase attention to unique issues faced by young women with

577   newly diagnosed breast cancer. *BMC Public Health*. 2015;15:37.

578   30. Babak MV, Ahn D. Modulation of Intracellular Copper Levels as the Mechanism of Action

579   of Anticancer Copper Complexes: Clinical Relevance. *Biomedicines*. 2021;9(8):852.

580   31. Blockhuys S. Defining the human copper proteome and analysis of its expression variation in

581   cancers. *Metallomics*. 2017;9(2):112-123.

582   32. Ishida S, Andreux P, Poitry-Yamate C, Auwerx J, Hanahan D. Bioavailable copper

583   modulates oxidative phosphorylation and growth of tumors. *Proc Natl Acad Sci USA*.

584   2013;110(48):19507-12.

585   33. Sha S, Si L, Wu X, et al. Prognostic analysis of cuproptosis-related gene in triple-negative

586   breast cancer. *Front Immunol*. 2022;13:922780.

587   34. Monteverde T, Sahoo S, La Montagna M, et al. CKAP2L Promotes Non–Small Cell Lung

588   Cancer Progression through Regulation of Transcription Elongation. *Cancer Research*.

589   2021;81(7):1719–1731.

590   35. Li Y-F, Tsai W-C, Chou C-H, et al. CKAP2L Knockdown Exerts Antitumor Effects by

591   Increasing miR-4496 in Glioblastoma Cell Lines. *IJMS*. 2020;22(1):197.

592   36. Sethi NS, Kikuchi O, Duronio GN, et al. Early TP53 alterations engage environmental

593   exposures to promote gastric premalignancy in an integrative mouse model. *Nat Genet*.

594   2020;52(2):219–230.

595   37. Aftab A, Shahzad S, Hussain HMJ, et al. CDKN2A/P16INK4A variants association with

596   breast cancer and their in-silico analysis. *Breast Cancer*. 2019;26(1):11–28.

597   38. Cheng T, Wu Y, Liu Z, et al. CDKN2A-mediated molecular subtypes characterize the

598   hallmarks of tumor microenvironment and guide precision medicine in triple-negative breast

599   cancer. *Front Immunol*. 2022;13:970950.

600   39. Ruiz NPE, Mohan V, Wu J, et al. Dynamic regulation of mitochondrial pyruvate metabolism

601   Is necessary for orthotopic pancreatic tumor growth. *Cancer Metab*. 2021;9(1):39.

602   40. Zhang F, Yan Y, Liang Q, et al. A combined analysis of bulk and single-cell sequencing data

603   reveals metabolic enzyme, pyruvate dehydrogenase E1 subunit beta (PDHB), as a prediction

604   biomarker for the tumor immune response and immunotherapy. *Heliyon*. 2023;9(2):e13456.

605   41. Huang Y, Xie F, Cheng X, et al. LncRNA MEG3 promotes endoplasmic reticulum stress and

606   suppresses proliferation and invasion of colorectal carcinoma cells through the MEG3/miR-

607   103a-3p/PDHB ceRNA pathway. *Neo*. 2021;68(2):362–374.

608   42. Shin D, Lee J, You JH, Kim D, Roh J-L. Dihydrolipoamide dehydrogenase regulates cystine

609   deprivation-induced ferroptosis in head and neck cancer. *Redox Biology*. 2020;30:101418.

610 43. Tsvetkov P, Coy S, Petrova B, et al. Copper induces cell death by targeting lipoylated TCA

611   cycle proteins. *Science.* 2022;375(6586):1254-1261.

612 44. Lampa M, Arlt H, He T, et al. Glutaminase is essential for the growth of triple-negative

613   breast cancer cells with a deregulated glutamine metabolism pathway and its suppression

614   synergizes with mTOR inhibition. *PLoS ONE.* 2017;12(9):e0185092.

615 45. Greene KS, Lukey MJ, Wang X, et al. SIRT5 stabilizes mitochondrial. glutaminase and

616   supports breast cancer tumorigenesis. *Proc Natl Acad Sci USA.* 2019;116(52):26625-26632

617 46. Yi X, Kim K, Yuan W, et al. Mice with heterozygous deficiency of lipoic acid synthase have

618   an increased sensitivity to lipopolysaccharide-induced tissue injury. *Journal of Leukocyte*

619   *Biology.* 2009;85(1):146-53.

620 47. Cai Y, He Q, Liu W, et al. Comprehensive analysis of the potential cuproptosis-related

621   biomarker LIAS that regulates prognosis and immunotherapy of pan-cancers. *Front Oncol.*

622   2022;12:952129.

623 48. Solmonson A, Faubert B, Gu W, et al. Compartmentalized metabolism supports midgestation

624   mammalian development. *Nature.* 2022;604(7905):349-353.

625 49. Chen Y, Xu T, Xie F, et al. Evaluating the biological functions of the prognostic genes

626   identified by the Pathology Atlas in bladder cancer. *Oncol Rep.* 2021;45(1):191-201.

627 50. Lv H, Liu X, Zeng X, et al. Comprehensive Analysis of Cuproptosis-Related Genes in

628   Immune Infiltration and Prognosis in Melanoma. *Front Pharmacol*. 2022;13:930041.

629 51. Heuchel R, Radtke F, Georgiev O, et al. The transcription factor MTF-1 is essential for basal

630   and heavy metal-induced metallothionein gene expression. *The EMBO Journal*.

631   1994;13(12):2870-5.

632 52. Peng W, zhu R, Zhou S, Mirzaei P, Mechref Y. Integrated Transcriptomics, Proteomics, and

633   Glycomics Reveals the Association between Up-regulation of Sialylated N-glycans/Integrin

634   and Breast Cancer Brain Metastasis. *Sci Rep*. 2019;9(1):17361.

635 53. Liu F, Zhang W, You X, et al. The oncoprotein HBXIP promotes glucose metabolism

636   reprogramming via downregulating SCO2 and PDHA1 in breast cancer. *Oncotarget*.

637   2015;6(29):27199-213.

638 54. Vousden KH, Ryan KM. p53 and metabolism. *Nat Rev Cancer*. 2009;9(10):691-700.

639 55. Kato T, Noma K, Ohara T, et al. Cancer-Associated Fibroblasts Affect Intratumoral CD8+

640   and FoxP3+ T Cells Via IL6 in the Tumor Microenvironment. *Clinical Cancer Research*.

641   2018;24(19):4820–4833.

642 56. Clark CE, Hingorani SR, Mick R, et al. Dynamics of the Immune Reaction to Pancreatic

643   Cancer from Inception to Invasion. *Cancer Research*. 2007;67(19):9518–9527.

644   57. Junjeong Choi, Jones Gyamfi, Haerin Jang, Ja Seung Koo. The role of tumor-associated

645   macrophage in breast cancer biology. *Histol Histopathol*. 2017;33(2):133–145.

646   58. Tawfik O, Kimler BF, Karnik T, Shehata P. Clinicopathological correlation of PD-L1

647   expression in primary and metastatic breast cancer and infiltrating immune cells. *Human*

648   *Pathology*. 2018;80:170–178.

649   59. Wang Y, Zhang Y, Hu K, et al. Elevated long noncoding RNA MALAT-1 expression is

650   predictive of poor prognosis in patients with breast cancer: a meta-analysis. *Bioscience*

651   *Reports*. 2020;40(8):BSR20200215.

652   60. Zahran A, Shaltout A, Fakhry H, et al. Prognostic Significance of Circulating CD28 Negative

653   Suppressor T Cells and Memory B Cells in Patients with Breast Cancer. *IranJImmunol*.

654   2020;17(2):95-110.

655   61. Bar I, Theate I, Haussy S, et al. MiR-210 Is Overexpressed in Tumor-infiltrating Plasma

656   Cells in Triple-negative Breast Cancer. *J Histochem Cytochem*. 2020;68(1):25-32.

657   62. Weng Y-S, Tseng H-Y, Chen Y-A, et al. MCT-1/miR-34a/IL-6/IL-6R signaling axis

658   promotes EMT progression, cancer stemness and M2 macrophage polarization in triple-

659   negative breast cancer. *Mol Cancer*. 2019;18(1):42.

660   63. Jerry DJ, Shull JD, Hadsell DL, et al. Genetic variation in sensitivity to estrogens and breast

661   cancer risk. *Mamm Genome*. 2018;29(1-2):24-37.

662   64. Parida S, Sharma D. The Microbiome–Estrogen Connection and Breast Cancer Risk. *Cells.*

663   2019;8(12):1642.

664   65. Lee YS, Ryu SW, Bae SJ, et al. Cross-platform meta-analysis of multiple gene expression

665   profiles identifies novel expression signatures in acquired anthracycline-resistant breast

666   cancer. *Oncology Reports.* 2015;33(4):1985-93.

667   66. Zhang W, Shen Y, Huang H, et al. A Rosetta Stone for Breast Cancer: Prognostic Value and

668   Dynamic Regulation of Neutrophil in Tumor Microenvironment. *Front Immunol.*

669   2020;11:1779.

670   67. Printz C. Investigational drug combined with chemotherapy improves response in patients

671   with BRCA-mutant breast cancer. *Cancer.* 2017;123(5):722-723.

672   68. Kulkoyluoglu-Cotul E, Arca A, Madak-Erdogan Z. Crosstalk between Estrogen Signaling

673   and Breast Cancer Metabolism. *Trends in Endocrinology & Metabolism.* 2019;30(1):25-38.

674   69. Kim H, Moon WK. Histological Findings of Mammary Gland Development and Risk of

675   Breast Cancer in *BRCA1* Mutant Mouse Models. *J Breast Cancer.* 2021;24(5):455-462.

676   70. Olivier DW, Pretorius E, Engelbrecht A-M. Serum amyloid A1: Innocent bystander or active

677   participant in cell migration in triple-negative breast cancer? *Experimental Cell Research.*

678   2021;406(1):112759.

679   71. Cao Z, Jin Z, Zeng L, et al. Prognostic and tumor-immune infiltration cell signatures in

680   tamoxifen-resistant breast cancers. *Gland Surg.* 2021;10(9):2766-2779.

681   72. Wang Z, Yang M-Q, Lei L, et al. Overexpression of KRT17 promotes proliferation and

682   invasion of non-small cell lung cancer and indicates poor prognosis. *CMAR.* 2019;11:7485-

683   7497.

684   73. Sarlos DP, Yusenko MV, Peterfi L, Szanto A, Kovacs G. Dual role of KRT17 : development

685   of papillary renal cell tumor and progression of conventional renal cell carcinoma. *J Cancer.*

686   2019;10(21):5124-5129.

687   74. Chivu-Economescu M, Dragu DL, Necula LG, et al. Knockdown of KRT17 by siRNA

688   induces antitumoral effects on gastric cancer cells. *Gastric Cancer.* 2017;20(6):948-959.

689   75. Jinesh GG, Flores ER, Brohl AS. Chromosome 19 miRNA cluster and CEBPB expression

690   specifically mark and potentially drive triple negative breast cancers. *PLoS ONE.*

691   2018;13(10):e0206008.

692   76. Wu J, Xu H, Ji H, et al. Low Expression of Keratin17 is Related to Poor Prognosis in Bladder

693   Cancer. *OTT.* 2021;14:577-587.

694   77. Han W, Hu C, Fan Z-J, Shen G-L. Transcript levels of keratin 1/5/6/14/15/16/17 as potential

695   prognostic indicators in melanoma patients. *Sci Rep.* 2021;11(1):1023.

696   78. Jiang K, Lu Q, Li Q, Ji Y, Chen W, Xue X. Astragaloside IV inhibits breast cancer cell

697   invasion by suppressing Vav3 mediated Rac1/MAPK signaling. *International*

698   *Immunopharmacology.* 2017;42:195-202.

699   79. Lee K, Liu Y, Mo JQ, Zhang J, Dong Z, Lu S. Vav3 oncogene activates estrogen receptor

700   and its overexpression may be involved in human breast cancer. *BMC Cancer.* 2008;8:158.

701   80. Yang B, Ma C, Chen Z, et al. Correlation of Immunoglobulin G Expression and Histological

702   Subtype and Stage in Breast Cancer. *PLoS ONE.* 2013;8(3):e58706.

703   81. Syed P, Gupta S, Choudhary S, et al. Autoantibody Profiling of Glioma Serum Samples to

704   Identify Biomarkers Using Human Proteome Arrays. *Sci Rep.* 2015;5:13895.

705   82. Chu J, Li Y, Deng Z, et al. IGHG1 Regulates Prostate Cancer Growth via the MEK/ERK/c-

706   Myc Pathway. *BioMed Research International.* 2019;2019:7201562.

707   83. Ribieras S, Tomasetto C, Rio M-C. The pS2/TFF1 trefoil factor, from basic research to

708   clinical applications. *Biochimica et Biophysica Acta (BBA) - Reviews on Cancer.*

709   1998;1378(1):F61-77.

710   84. Perry JK, Kannan N, Grandison PM, Mitchell MD, Lobie PE. Are trefoil factors oncogenic?

711   *Trends in Endocrinology & Metabolism.* 2008;19(2):74-81.

712   85. Corte MD, Tamargo F, Alvarez A, et al. Cytosolic levels of TFF1/pS2 in breast cancer: their

713   relationship with clinical–pathological parameters and their prognostic significance. *Breast*

714   *Cancer Res Treat.* 2006;96(1):63-72.

715   86. Buache E, Etique N, Alpy F, et al. Deficiency in trefoil factor 1 (TFF1) increases

716   tumorigenicity of human breast cancer cells and mammary tumor development in TFF1-

717   knockout mice. *Oncogene.* 2011;30(29):3261-73.

718   87. Ni J, Peng Y, Yang F-L, Xi X, Huang X-W, He C. Overexpression of CLEC3A promotes

719   tumor progression and poor prognosis in breast invasive ductal cancer. *OTT.* 2018;11:3303-

720   3312.

721   88. Bakaeean B, Gholamin M, Yazdi SAT, et al. Novel Biomarkers Aim at Detecting Metastatic

722   Sentinel Lymph Nodes in Breast Cancer. *Ibj.* 2020;24(3):183-91.

723   89. Uras IZ, Moll HP, Casanova E. Targeting KRAS Mutant Non-Small-Cell Lung Cancer: Past,

724   Present and Future. *IJMS.* 2020;21(12):4325.

725   90. Luo J. KRAS mutation in pancreatic cancer. *Seminars in Oncology.* 2021;48(1):10–18.

726   91. Tokumaru Y, Oshi M, Katsuta E, et al. KRAS signaling enriched triple negative breast

727   cancer is associated with favorable tumor immune microenvironment and better survival. *Am*

728   *J Cancer Res.* 2020;10(3):897-907.

729   92. Ribatti D, Annese T, Tamma R. Controversial role of mast cells in breast cancer tumor

730   progression and angiogenesis. *Clinical Breast Cancer*. 2021;21(6):486–491.

731   93. Chong ZX, Yeap SK, Ho WY. Angiogenesis regulation by microRNAs and long non-coding

732   RNAs in human breast cancer. *Pathology - Research and Practice*. 2021;219:153326.

733   94. Steinberg F, Röhrborn HJ, Otto T, et al. NIR Reflection Measurements of Hemoglobin and

734   Cytochrome aa3 in Healthy Tissue and Tumors. Correlations to oxygen consumption:

735   preclinical and clinical data. *Adv Exp Med Biol*. 1997;428:69-77.

736   95. Boneberg E-M, Legler DF, Hoefer MM, et al. Angiogenesis and lymphangiogenesis are

737   downregulated in primary breast cancer. *Br J Cancer*. 2009;101(4):605–614.

738   96. Lu Y, Ding Y, Wei J, et al. Anticancer effects of Traditional Chinese Medicine on epithelial-

739   mesenchymal transition (EMT) in breast cancer: Cellular and molecular targets. *European

740   Journal of Pharmacology*. 2021;907:174275.

741   97. Vardas V, Politaki E, Pantazaka E, Georgoulias V, Kallergi G. Epithelial-to-mesenchymal

742   transition of tumor cells: cancer progression and metastasis. *Int J Dev Biol*. 2022;66(1-2-

743   3):277–283.

744   98. Kar R, Jha NK, Jha SK, et al. A "NOTCH" Deeper into the Epithelial-To-Mesenchymal

745   Transition (EMT) Program in Breast Cancer. *Genes*. 2019;10(12):961.

746   99. Oshi M, Takahashi H, Tokumaru Y, et al. G2M Cell Cycle Pathway Score as a Prognostic

747   Biomarker of Metastasis in Estrogen Receptor (ER)-Positive Breast Cancer. *IJMS*.

748   2020;21(8):2921.

749   100. Huang H-W, Tang J-Y, Ou-Yang F, et al. Sinularin Selectively Kills Breast Cancer Cells

750   Showing G2/M Arrest, Apoptosis, and Oxidative DNA Damage. *Molecules*. 2018;23(4):849.

751   101. Mehdipour F, Razmkhah M, Hosseini A, et al. Increased B Regulatory Phenotype in Non-

752   Metastatic Lymph Nodes of Node-Positive Breast Cancer Patients. *Scand J Immunol*.

753   2016;83(3):195-202.

754   102. Poncin A, Onesti CE, Josse C, et al. Immunity and Breast Cancer: Focus on Eosinophils.

755   *Biomedicines*. 2021;9(9):1087.

756   103. Ali HR, Chlon L, Pharoah PDP, Markowetz F, Caldas C. Patterns of Immune Infiltration in

757   Breast Cancer and Their Clinical Implications: A Gene-Expression-Based Retrospective

758   Study. *PLoS Med*. 2016;13(12):e1002194.

759   104. Lotfinejad P, Kazemi T, Safaei S, et al. PD-L1 silencing inhibits triple-negative breast

760   cancer development and upregulates T-cell-induced pro-inflammatory cytokines.

761   *Biomedicine & Pharmacotherapy*. 2021;138:111436.

762   105. Schütz F, Stefanovic S, Mayer L, von Au A, Domschke C, Sohn C. PD-1/PD-L1 Pathway

763   in Breast Cancer. *Oncol Res Treat*. 2017;40(5):294-297.

764   106. Sha S, Si L, Wu X, et al. Prognostic analysis of cuproptosis-related gene in triple-negative

765   breast cancer. *Front Immunol.* 2022;13:922780.

766   **Figure legends**

767   **FIGURE 1 | The expression of ten cuproptosis genes in BRCA. (A-B)** The GO and KEGG

768   functional enrichment analysis of 10 cuproptosis genes. **(C)** Somatic mutational analysis of 10

769   cuproptosis genes in BRCA samples. **(D)** The expression trends of 10 cuproptosis genes in

770   BRCA. * p<0.05, ** p<0.01, **** p<0.0001.

771

772   **FIGURE 2 | Recognition of cuproptosis-associated subtypes of BRCA. (A)** UMAP reduced

773   dimensional analysis for three cuproptosis-related subtypes. **(B)** Kaplan-Meier curves of three

774   cuproptosis-related subtypes. **(C-H)** Correlation analysis of three cuproptosis-related subtypes

775   with clinical factors.

776

777   **FIGURE 3 | TME analysis of cuproptosis-associated subtypes of BRCA. (A-D)** Immune

778   score, stromal score, ESTIMATE score, and tumor purity differences in three cuproptosis-related

779   subtypes. **(E-F)** The fraction of 28 immune gene sets for three cuproptosis-associated subtypes.

780   **(G)** Differential infiltration levels of 22 immune cell types in three cuproptosis-associated

781   subtypes. ns: not significant, * p<0.05, ** p<0.01, *** p<0.001, **** p<0.0001.

782

783 **FIGURE 4 | The cuproptosis-associated DEGs in BRCA. (A)** The Venn diagram to gain the

784 cuproptosis-associated DEGs in BRCA. **(B)** Heatmap of the correlations between 38 intersecting

785 genes and 10 cuproptosis-related genes. ** represents P < 0.01. **(C)** The results of functional

786 enrichment analysis of 38 cuproptosis-associated DEGs in BRCA. **(D)** Distribution of clinical

787 characteristics of five clustered subtypes and expression of 38 DEGs associated with cuproptosis.

788 **(E)** Survival analysis among the five subtypes.

789

790 **FIGURE 5 | The cuproptosis-relevant prognostic signature in BRCA. (A)** The forest plot of

791 6 cuproptosis-associated genes significantly linked to OS in BRCA. **(B)** Survival rate

792 comparison between high- and low-Cusig score groups. **(C)** The correlation between different

793 subtypes and high- and low-Cusig scores. **(D)** Differences in Cusig scores between the five

794 BRCA subtypes based on 38 cuproptosis-associated DEGs. **(E)** Prognostic validation of high-

795 and low-Cusig score groups in GSE42568 dataset. **(F)** Prognostic validation of high- and low-

796 Cusig score groups in GSE20711 dataset.

797

798 **FIGURE 6 | The functional enrichment analysis between high- and low-Cusig score**

799 **samples. (A-B)** The GSVA analysis of high- and low-Cusig score groups based on Hallmark and

800 KEGG gene sets. **(C)** The top 10 GO- BP entries enriched by DEGs between high- and low-

801 Cusig score groups. **(D)** The top 5 enriched entries in the high- and low-Cusig score group.

802

803 **FIGURE 7 | Association of cuproptosis-relevant prognostic signature with TME. (A-D)**

804 Trends in immune score, stromal score, estimated score and tumour purity for high- and low-

805 Cusig score groups. **(E)** The fraction of different immune cell infiltrations in high- and low-

806 Cusig score groups. **(F-G)** The comparison of PD-L1 and immunophenotype scores in high- and

807 low-Cusig score groups. **(H)** The TIDE value of high and low Cusig score groups.

808

809 **FIGURE 8 | The mutation landscape analysis. (A)** The somatic mutations in high-Cusig score

810 samples. **(B)** The somatic mutations in low-Cusig score samples. **(C)** The analysis of copy

811 number variation in groups with high- and low-Cusig scores.

812

813 **FIGURE 9 | The expression of prognostic genes in cell lines detected by RT-qPCR. (A)**

814 CLEC3A **(B)** KRT17 **(C)** SAA1 **(D)** TFF1 **(E)** IGHG1 **(F)** VAV3 * p<0.05, ** p<0.01, ***

815 p<0.001, **** p<0.0001.

Figure 1

The expression of ten cuproptosis genes in BRCA.

(A-B) The GO and KEGG functional enrichment analysis of 10 cuproptosis genes. **(C)** Somatic mutational analysis of 10 cuproptosis genes in BRCA samples. **(D)** The expression trends of 10 cuproptosis genes in BRCA. * p<0.05, ** p<0.01, **** p<0.0001.

Figure 2

Recognition of cuproptosis-associated subtypes of BRCA.

(A) UMAP reduced dimensional analysis for three cuproptosis-related subtypes. **(B)** Kaplan-Meier curves of three cuproptosis-related subtypes. **(C-H)** Correlation analysis of three cuproptosis-related subtypes with clinical factors.
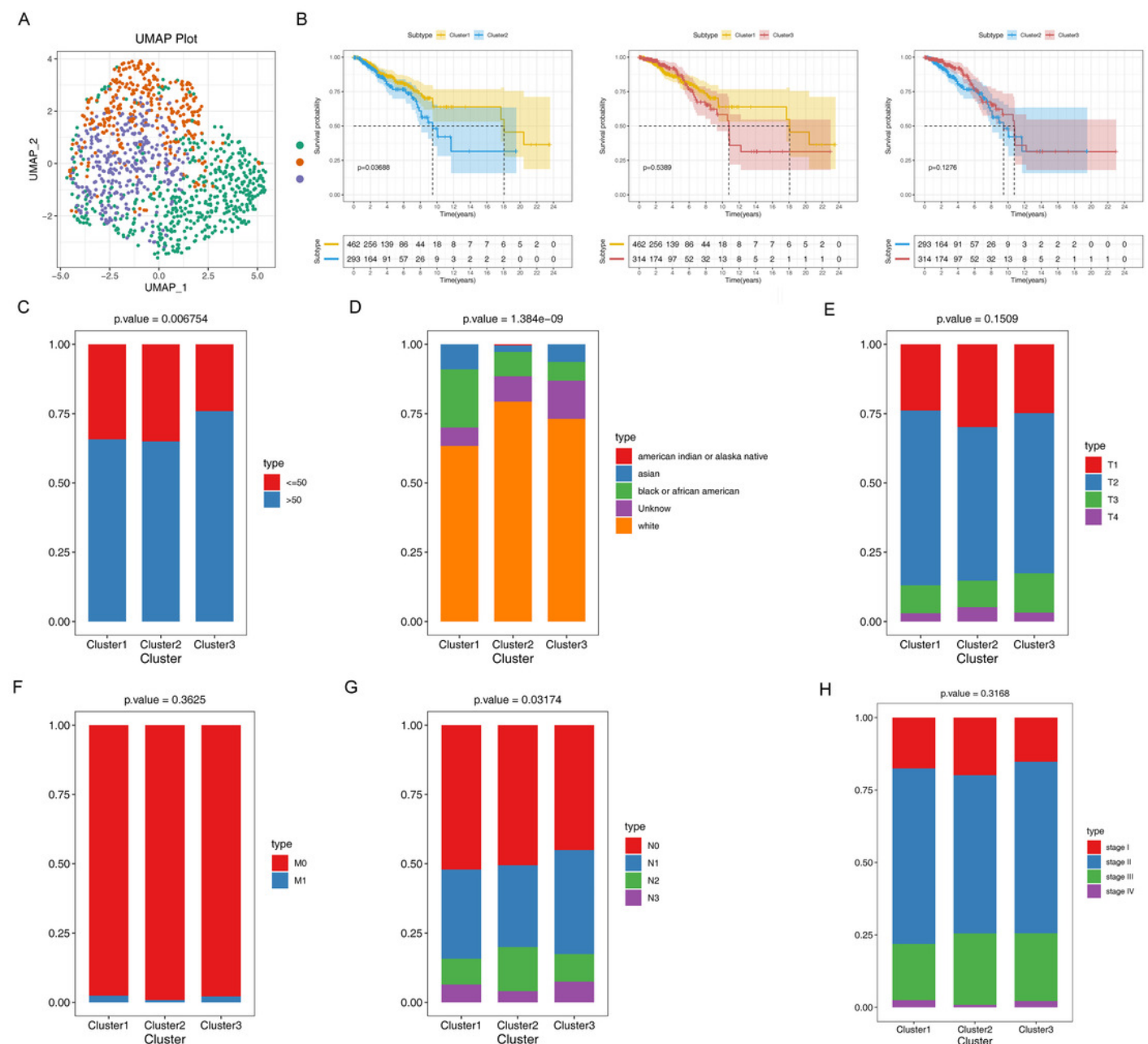
Figure 3

TME analysis of cuproptosis-associated subtypes of BRCA.

(A-D) Immune score, stromal score, ESTIMATE score, and tumor purity differences in three cuproptosis-related subtypes. **(E-F)** The fraction of 28 immune gene sets for three cuproptosis-associated subtypes. **(G)** Differential infiltration levels of 22 immune cell types in three cuproptosis-associated subtypes. ns: not significant, * p<0.05, ** p<0.01, *** p<0.001, **** p<0.0001.
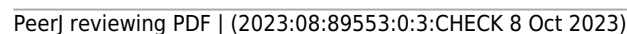
Figure 4

The cuproptosis-associated DEGs in BRCA.

(A) The Venn diagram to gain the cuproptosis-associated DEGs in BRCA. (B) Heatmap of the correlations between 38 intersecting genes and 10 cuproptosis related genes. ** represents P < 0.01. (C) The results of functional enrichment analysis of 38 cuproptosis-associated DEGs in BRCA. (D) Distribution of clinical characteristics of five clustered subtypes and expression of 38 DEGs associated with cuproptosis. (E) Survival analysis among the five subtypes.
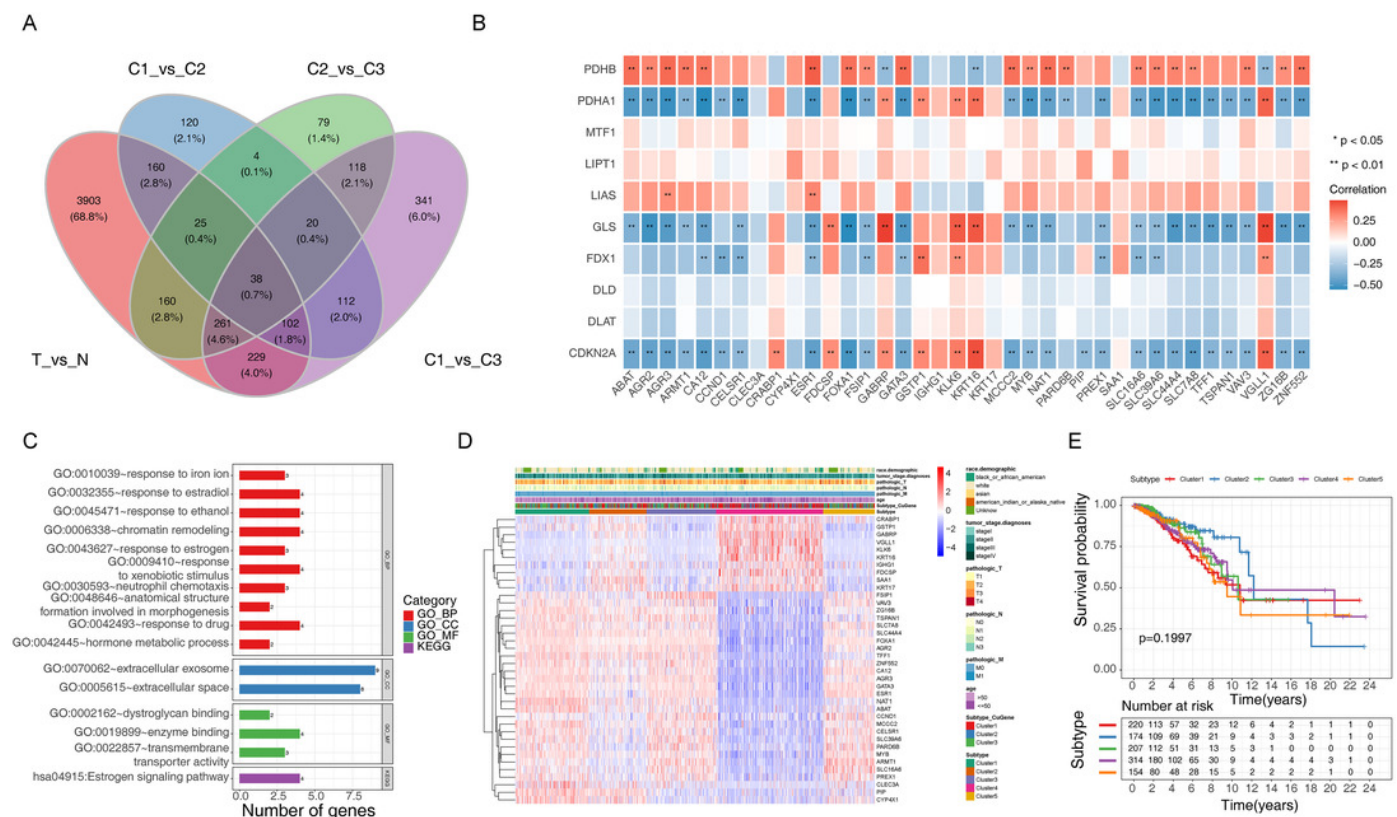
Figure 5

The cuproptosis-relevant prognostic signature in BRCA.

(A) The forest plot of 6 cuproptosis-associated genes significantly linked to OS in BRCA. **(B)** Survival rate comparison between high- and low-Cusig score groups. **(C)** The correlation between different subtypes and high- and low-Cusig score **(D)** Differences on Cusig scores between the five BRCA subtypes based on 38 cuproptosis-associated DEGs. **(E)** Prognostic validation of high- and low-Cusig score groups in GSE42568 dataset. (**F**) Prognostic validation of high- and low-Cusig score groups in GSE20711 dataset.
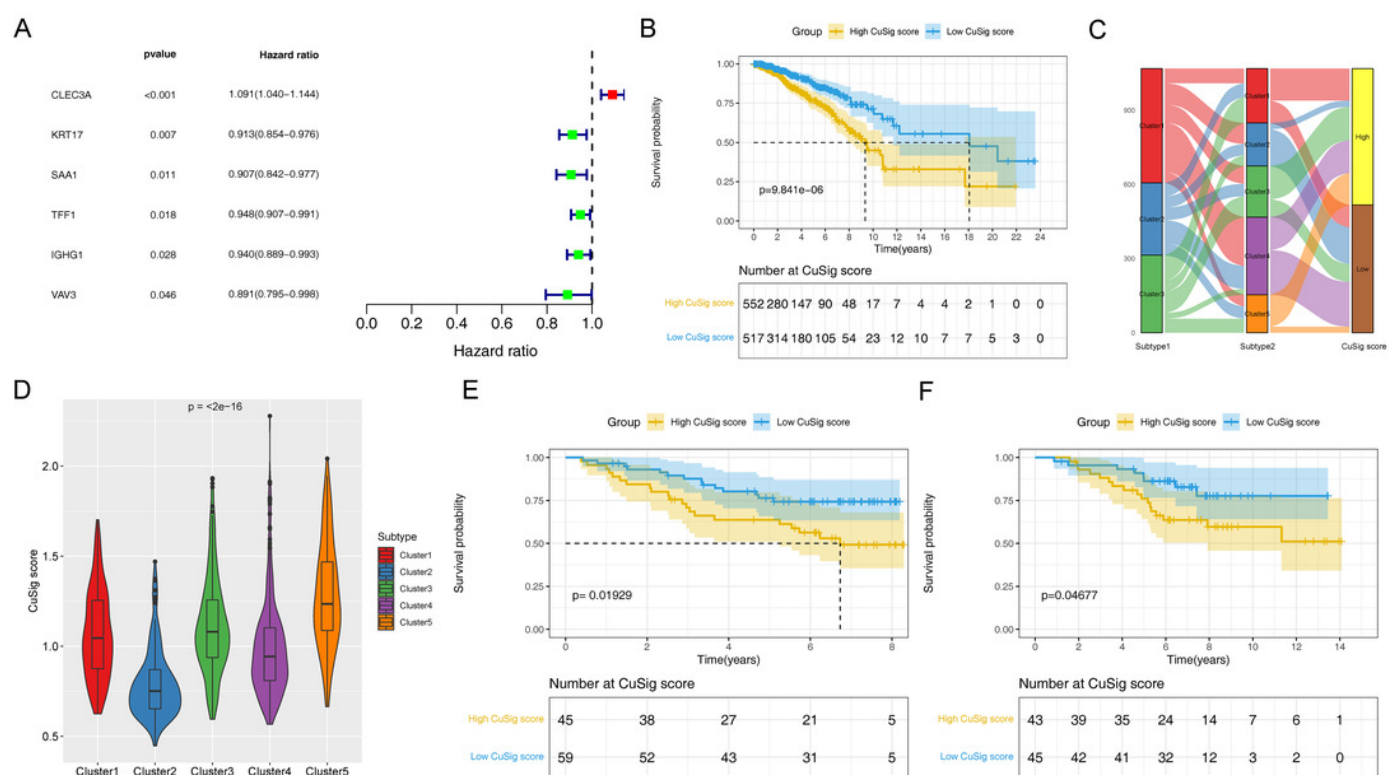
Figure 6

The functional enrichment analysis between high- and low-Cusig score samples.

(A-B) The GSVA analysis of high- and low-Cusig score groups based on Hallmark and KEGG gene sets. **(C)** The top 10 GO- BP entries enriched by DEGs between high- and low-Cusig score groups. **(D)** The top 5 enriched entries in the high- and low-Cusig score group.
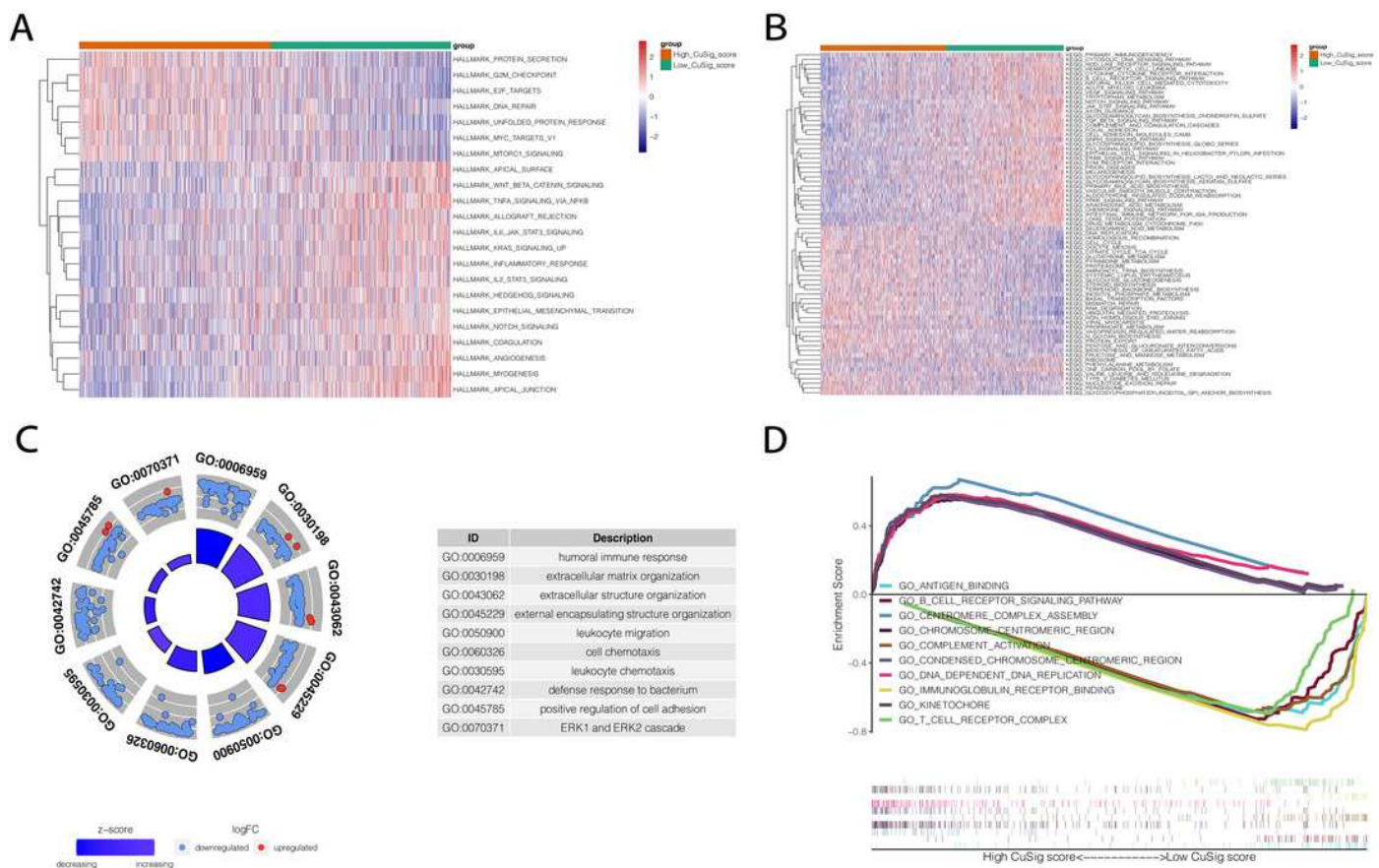
Figure 7

Association of cuproptosis-relevant prognostic signature with TME.

(A-D) Trends in immune score, stromal score, estimated score and tumour purity for high- and low-Cusig score groups. **(E)** The fraction of different immune cell infiltrations in high- and low-Cusig score groups. **(F-G)** The comparison of PD-L1 and immunophenotype scores in high- and low-Cusig score groups. **(H)** The TIDE value of high and low Cusig score groups.
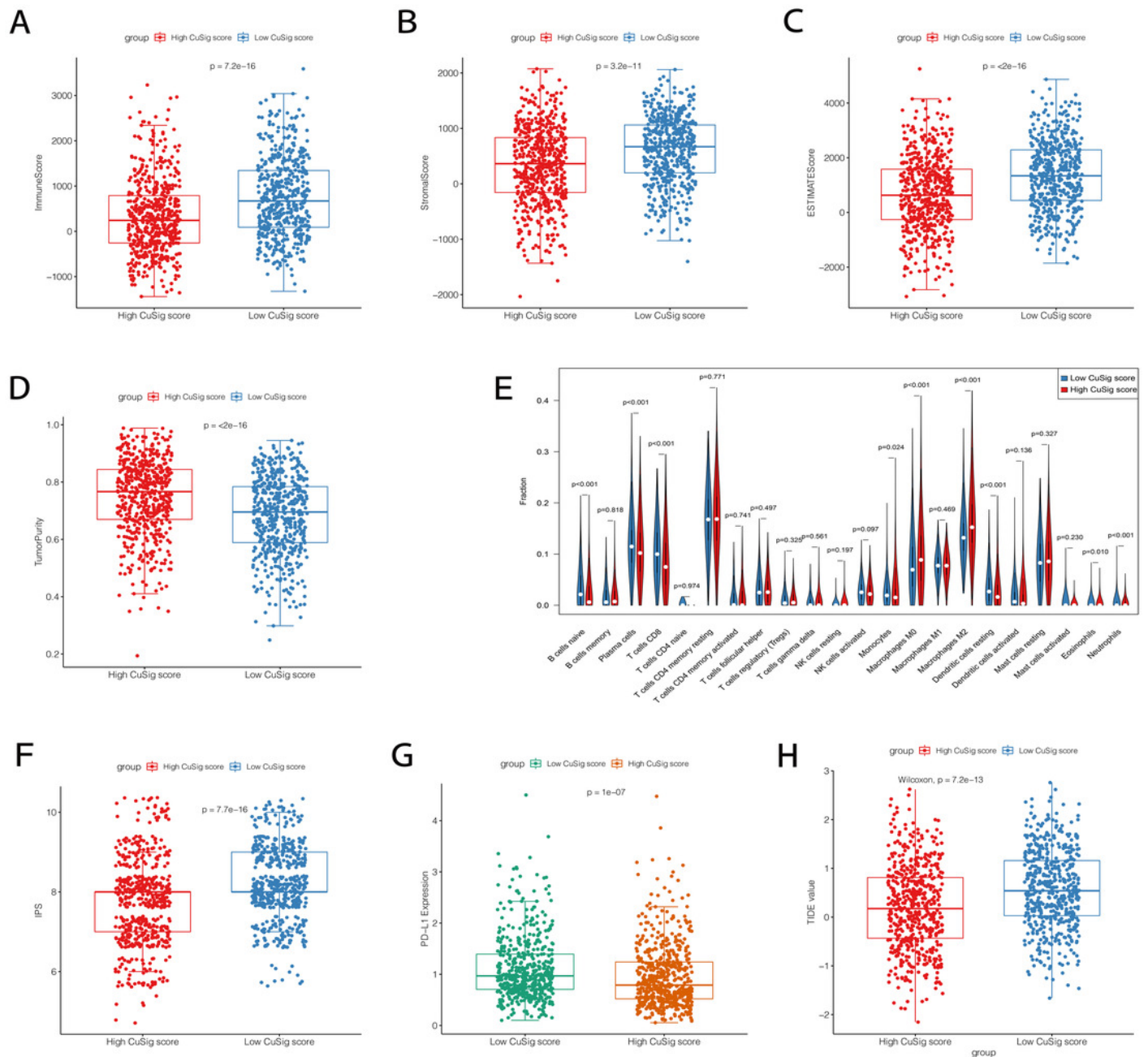
Figure 8

The mutation landscape analysis.

(A) The somatic mutations in high-Cusig score samples. **(B)** The somatic mutations in low-Cusig score samples. **(C)** The analysis of copy number variation in groups with high- and low-Cusig scores.
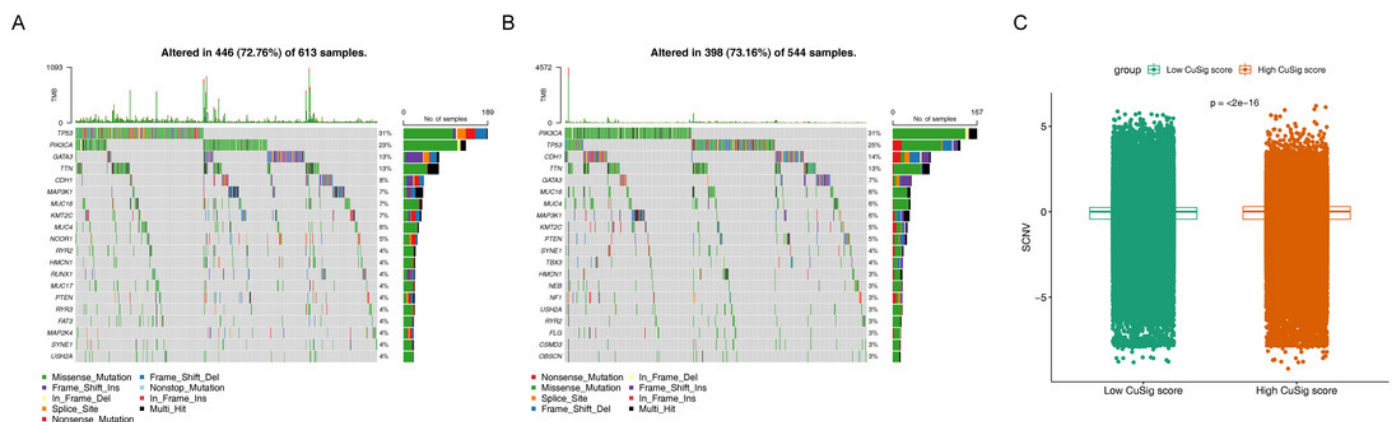
Figure 9

The expression of prognostic genes in cell lines detected by RT-qPCR.

(A) CLEC3A **(B)** KRT17 **(C)** SAA1 **(D)** TFF1 **(E)** IGHG1 **(F)** VAV3 * p<0.05, ** p<0.01, *** p<0.001, **** p<0.0001.
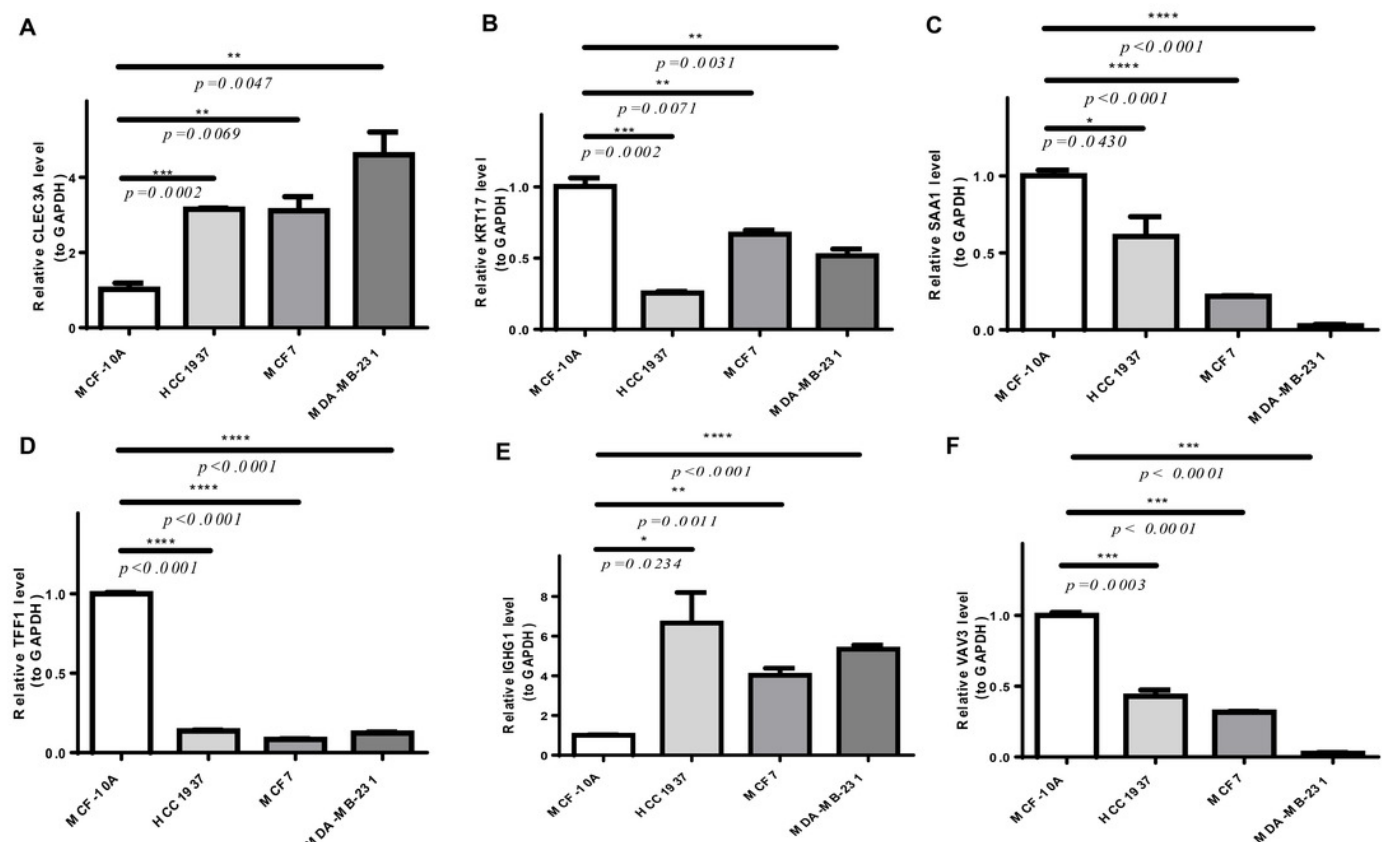
The sequences of the primers for qPCR.

The sequences of the primers for qPCR.

1 **Table 1 The primer sequences for qPCR**

primer	sequences
CLEC3A For	GGACTTGTAATTTGCATCCTGG
CLEC3A Rev	CTTGTGAACTTTAGTGCCTCGG
KRT17 For	GATGCCGAGGATTGGTTCTT
KRT17 Rev	TCTCTGTCTCCGCCAGGTTG
SAA1 For	GGTTTTCTGCTCCTTGGTCCT
SAA1 Rev	AGCCGATGTAATTGGCTTCTC
TFF1 For	CCCTCCCAGTGTGCAAATAAG
TFF1 Rev	GAACGGTGTCGTCGAAACAG
IGHG1 For	CTGGCTGAATGGCAAGGAGTA
IGHG1 Rev	GCGATGTCGCTGGGATAGAAG
VAV3 For	ACATTCTTTCAGAACAAGGGAC
VAV3 Rev	GAATAATCTACTGGTTTGGGCAC
GAPDH For	CCCATCACCATCTTCCAGG
GAPDH Rev	CATCACGCCACAGTTTCCC